
Relieving the Plateau: Active Semi-Supervised Learning for a Better Landscape

Seo Taek Kong Soomin Jeon Jaewon Lee Hongseok Lee Kyu-Hwan Jung

Vuno Inc.
kyuhwanjung@gmail.com

Abstract

Deep learning (DL) relies on massive amounts of labeled data, and improving its labeled sample-efficiency remains one of the most important problems since its advent. Semi-supervised learning (SSL) leverages unlabeled data that are more accessible than their labeled counterparts. Active learning (AL) selects unlabeled instances to be annotated by a human-in-the-loop in hopes of better performance with less labeled data. Given the accessible pool of unlabeled data in pool-based AL, it seems natural to use SSL when training and AL to update the labeled set; however, algorithms designed for their combination remain limited. In this work, we first prove that convergence of gradient descent on sufficiently wide ReLU networks can be expressed in terms of their Gram matrix' eigen-spectrum. Equipped with a few theoretical insights, we propose convergence rate control (CRC), an AL algorithm that selects unlabeled data to improve the problem conditioning upon inclusion to the labeled set, by formulating an acquisition step in terms of improving training dynamics. Extensive experiments show that SSL algorithms coupled with CRC can achieve high performance using very few labeled data.

1 Introduction

The data-hungry nature of supervised deep learning (DL) algorithms has spurred interest in active learning (AL), where a model can interact with a dedicated annotator and request unlabeled instances to be labeled. In the pool-based AL setting, a model has access to a fixed set of unlabeled samples and can select those which need be labeled for training. Under certain conditions on the task, AL can provably achieve up to exponential improvements in sample complexity and thus has great potential for reducing the number of labeled instances required to achieve high accuracy. This is especially important when the annotation task is extremely costly, for example in medical imaging where only highly-specialized experts can diagnose a subject's condition.

Active learning algorithms have been extensively explored, with various formulations including uncertainty-based sampling (Wang & Shang, 2014), aligning the labeled and unlabeled distributions (Gissin & Shalev-Shwartz, 2019) with connections to domain adaptation (Ben-David et al., 2010), and coreset (Sener & Savarese, 2017). Furthermore, there is no standard method in modeling a deep neural network's (DNN) uncertainty, and uncertainty-based AL has its own variants ranging from utilizing Bayesian networks (Kirsch et al., 2019) to using a model's predictive confidence (Wang & Shang, 2014). This ambiguous characterization of how much information a sample's label carries also inspired AL algorithms to maximize the expected change of a classification model (Huang et al., 2016; Ash et al., 2020).

While AL comes with optimistic potentials, most algorithms outperform random sampling (passive learning) by only a small margin, with follow-up works (Gissin & Shalev-Shwartz, 2019; Sener & Savarese, 2017; Ducoffe & Precioso, 2018) reporting worse performance of certain AL algorithms than random sampling due to their dependency on specific model architectures or dataset characteristics. Furthermore, the performance of AL algorithms are usually reported by training a model using supervised learning (SL) on the queried labeled data despite the availability of unlabeled data in pool-based AL. Semi-supervised learning (SSL) has recently shown impressive performance with a small number of labeled instances, and its most premature variant known as pseudo-labeling (Lee, 2013) has been combined with AL algorithms (Wang et al., 2016). One recent work (Song et al., 2019) uses a rather modern SSL algorithm (Berthelot et al., 2019) and shows the strength of combining AL with SSL which we name ASSL. However, their algorithm is not designed specifically considering the ASSL setting.

In this work, we propose a novel AL strategy which we call convergence rate control (CRC), and show that CRC can rapidly achieve the high performance of fully-supervised algorithms using far less labeled data. CRC is inspired by recent developments in DNN theory, namely the neural tangent kernel (NTK) (Jacot et al., 2018), and is essentially a kernel-based sampling strategy that remains under-explored in DL-based AL. In addition to establishing a baseline for existing AL algorithms in realistic SSL settings (Oliver et al., 2018), our experiments demonstrate the superiority of CRC to other DL-based approaches to AL when coupled with seminal (Tarvainen & Valpola, 2017) and state-of-the-art (Sohn et al., 2020) SSL algorithms. Because SSL algorithms already attain high performance with substantially fewer data than that required for SL, we focus on the low data-regime where even SSL algorithms have room for improvement.

2 Optimization in Deep Learning

2.1 Semi-supervised Learning and Active Learning

In contrast to the $\tilde{\Theta}(\frac{1}{\epsilon})$ i.i.d labeled samples necessary and sufficient for attaining ϵ -classification error for realizable datasets Lopez-Paz et al. (2016); Massart & Nédélec (2006), a few works show that both SSL and AL can provably attain substantial sample complexity gains under restrictive settings. One example constructed by Göpfert et al. (2019) illustrates how $O(\log 1/\epsilon)$ labeled and $O(1/\epsilon^2)$ unlabeled samples suffice to attain the same error level. Considering the $\epsilon \approx 6\%$ error achieved by fully-supervised learning in CIFAR10 using $O(1/\epsilon) \approx 50,000$ labeled samples, SSL with only $O(\text{poly log}(1/\epsilon)) \approx 250$ labeled and $O(1/\epsilon) \approx 49,750$ unlabeled samples is analogous to the above SSL example (with a slightly higher error due to $\epsilon^2 \rightarrow \epsilon$). FixMatch (Sohn et al., 2020) is a recently proposed SSL algorithm that nearly obtains this sample efficiency in real-world datasets although the conditions in Göpfert et al. (2019) on the underlying distributions are clearly violated. In contrast, Balcan et al. (2010) suggests optimistic gains should be achievable by AL under different but similarly restrictive conditions on the task whereas in practice this is far from what is observed.

State-of-the-art SSL algorithms impose consistency constraints on the function, restricting well-optimized models $f^{(\infty)}$ to those that generalize well: small $\|f^{(\infty)} - f^*\|$ where $f^* = \arg \min_f \mathbb{E}[\mathcal{L}_n(f)]$ is the optimal classifier and \mathcal{L}_n is the empirical loss over n samples. Given a fixed budget to annotate data, we would like to simultaneously minimize the optimization and asymptotic-generalization error $\|f^{(T)} - f^{(\infty)}\| + \|f^{(\infty)} - f^*\| \geq \|f^{(T)} - f^*\|$. The two optimization and asymptotic-generalization terms are not necessarily independent, for example in the online setting where less training iterations (hence fewer samples observed) implies better generalization, $f^{(\infty)} = f^*$. Local landscapes near critical points are often coined with generalization (He et al., 2019), further demonstrating an intimate relationship between optimization and generalization. Throughout training, Athiwaratkun et al. (2019) observed that SGD steps on the induced Lagrangian takes large steps, and better optimization could further improve SSL performances. Encompassing these objectives, we later cast an acquisition step as an optimization problem minimizing $\|f^{(T)} - f^{(\infty)}\|$ and utilize SSL to enforce small $\|f^{(\infty)} - f^*\|$.

2.2 Neural Tangent Kernel

The neural tangent kernel (NTK) (Jacot et al., 2018) is a theoretical tool developed to understand the success of gradient descent (GD) in training DNNs by analyzing their infinite-width limit. In particular, the dynamics of infinitesimal-GD on a DNN f_{θ_t} follows a closed form expression

$$\frac{df_{\theta_t}(\mathcal{X})}{dt} = -\hat{\mathcal{K}}^{(t)}(\mathcal{X}, \mathcal{X}) (f_{\theta_t}(\mathcal{X}) - \mathcal{Y}). \quad (1)$$

when minimizing the mean-squared error (MSE) loss, where $\hat{\mathcal{K}}^{(t)}(\mathcal{X}, \mathcal{X}) = [\nabla_{\theta} f_{\theta_t}(x)^T \nabla_{\theta} f_{\theta_t}(x')]_{(x, x') \in \mathcal{X} \times \mathcal{X}}$ is known as the empirical NTK or model’s Gram matrix (Arora et al., 2019; Du et al., 2019), each element $\nabla_{\theta} f_{\theta_t}(x)^T \nabla_{\theta} f_{\theta_t}(x') \in \mathbb{R}^{C \times C}$ is a matrix block, and C is the number of classes.

Properly initialized infinite-width networks satisfy a remarkable property: the training dynamics of GD can be characterized by a matrix \mathcal{K} independent of time, namely the NTK:

$$\frac{df_{\theta_t}(\mathcal{X})}{dt} = -\mathcal{K}(\mathcal{X}, \mathcal{X}) (f_{\theta_t}(\mathcal{X}) - \mathcal{Y}), \quad (2)$$

which holds with high probability over random initialization. Assuming a network that satisfies the differential equation, the transient solution is given by

$$f_{\theta_t}(\mathcal{X}) = \sum_i c_i v_i \exp(-\lambda_i(\mathcal{X})t) \quad (3)$$

for some constants c_i and eigenvalue/vector pairs (λ_i, v_i) of the NTK $\mathcal{K}(\mathcal{X}, \mathcal{X})$. Notice how the NTK, and in turn the convergence rate, depends on the set of instances \mathcal{X} it is computed over. This sparks the intuition that the rate of convergence can be *controlled* by carefully constructing the labeled set.

2.3 Convergence for Finite-Width Networks

The above intuition based on the NTK carries on to finite-width networks. Optimizing DNNs can be extremely difficult, and basic principles suggest that if an algorithm converges, its rate can be expressed in terms of the problem’s conditioning. The goal of this section is not to show the fastest rate of convergence of GD for DNNs, but to show that convergence in terms of a ReLU network’s Gram matrix’ minimum eigenvalue is implied by properties of ReLU networks demonstrated by Allen-Zhu et al. (2019). For simplicity of exposition, consider 1-dimensional outputs ($C = 1$). We override notation for the MSE loss at time t as $\mathcal{L}_t = \mathcal{L}(\theta_t)$ whenever necessary. For only this section, we assume a non-degenerate training set $\|x_i - x_j\| \geq \delta, \forall i, j$ as common in DNN analysis. Proofs and detailed expressions in the statements are deferred to the Appendix.

A common overparametrization argument (Lee et al., 2019; Du et al., 2019; Allen-Zhu et al., 2019) is that sufficiently wide networks trained with GD lie near initialization. Convergence of GD then reduces to proving desirable conditions of the loss function within this regime. Allen-Zhu et al. (2019) prove that there is ‘no critical point’ and that the loss function is semi-smooth near initialization for ReLU networks. However, they also show empirically that finite-width networks used in practice often escape the initialization’s neighborhood, but still satisfies conditions for GD’s convergence which partially explains the success of GD-based optimization. Alternatively, Du et al. (2019) express the training dynamics as a function of the empirical NTK and perturbation terms.

Lemma 1. *For any DNN architecture with once-differentiable activation functions, gradient descent on the MSE loss \mathcal{L}_t with step size η follows the recursive relation:*

$$\mathcal{L}_{t+1} \leq \left(1 - \eta \lambda_{\min}(\hat{\mathcal{K}}_t)\right) \mathcal{L}_t + \xi_t + \epsilon_t, \quad (4)$$

where $\xi_t = \int_0^\eta \nabla \mathcal{L}_t^T (\nabla \mathcal{L}_t - \nabla \mathcal{L}(\theta_t - \gamma \nabla \mathcal{L}_t)) d\gamma$ and $\epsilon_t = \frac{1}{2}(f_{\theta_{t+1}} - f_{\theta_t})^2$.

The authors go on to show that for a class of DNNs that does not encompass ReLU networks, the perturbation term behaves linearly $\xi_t + \epsilon_t \sim \eta^2 \mathcal{L}_t$ with respect to the loss function, and that the empirical and true NTKs have similar eigendistributions. Consequently, $\lambda_{\min}(\hat{\mathcal{K}}_t)$ can be replaced

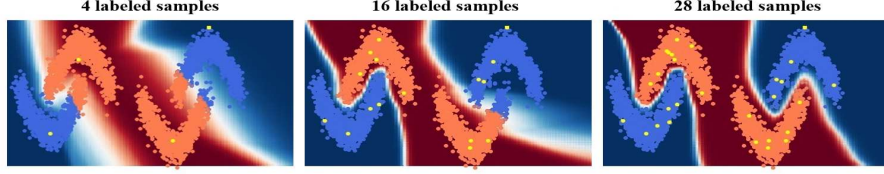


Figure 1: Illustration of how Π -model’s (Laine & Aila, 2017) decision boundary changes as the proposed algorithm enlarges the labeled set. The 4 initial pivot points were manually selected.

with a constant multiple of the time-independent term $\lambda_{\min}(\mathcal{K})$, and the loss function is a geometrically decreasing sequence bounded below, implying convergence.

Here we show that $\xi_t + \epsilon_t$ behaves linearly w.r.t \mathcal{L}_t for sufficiently wide *ReLU networks*. First, we recall an extended notion of smoothness used in optimization.

Definition 1 (Smoothness). *A non-negative, once-differentiable function $g \in C^1(\mathcal{X})$ is (α, β) -smooth if*

$$g(y) \leq g(x) + \nabla g(x)^T(y - x) + \alpha\sqrt{g(x)}\|y - x\| + \beta\|y - x\|^2 \quad (5)$$

for every $x, y \in \mathcal{X}$.

Another useful definition resembling convexity:

Definition 2 (Gradient Scale). *A non-negative function $g \in C^1(\mathcal{X})$ has gradients ∇g that scale as (μ, M) if*

$$\mu g(x) \leq \|\nabla g(x)\|^2 \leq M g(x), \forall x \in \mathcal{X}. \quad (6)$$

If a function’s gradients scale as (μ, M) , we say the gradient scale is bounded.

One difficulty in applying the techniques in (Du et al., 2019) to obtain bounds of the form in Eq. 4 for ReLU networks is that their proof relies on smooth and analytic activation functions. Instead, we show that the above smoothness and bounded gradient scale properties of wide ReLU networks (Allen-Zhu et al., 2019) are sufficient for the loss sequence in Eq. 4 to converge to zero. This may be of independent interest, as a direct comparison between convergence of ReLU by Allen-Zhu et al. (2019) and another class of activation functions in (Du et al., 2019) was unknown. Whereas the (α, β) -smoothness resembles Taylor’s intermediate theorem for traditional smoothness, Proposition 1 below shows that the extended notion can be expressed similarly to the Lipschitz continuity of gradients.

Proposition 1. *If g is (α, β) -smooth,*

$$\begin{aligned} & (\nabla g(y) - \nabla g(x))(y - x) \\ & \leq \alpha(\sqrt{g(x)} + \sqrt{g(y)})\|y - x\| + 2\beta\|y - x\|^2 \end{aligned}$$

We first state a condition that the MSE loss satisfies in a neighborhood of initialization for wide ReLU networks (Theorems 3 and 4 in Allen-Zhu et al.).

Condition 1. *A loss \mathcal{L} is (α, β) -smooth and its gradients scale as (μ, M) .*

Lemma 2. *If $\mathcal{L}_t := \mathcal{L}(\theta_t)$ satisfies Condition 2, we have*

$$\begin{aligned} \xi_t & \leq \mathcal{O}(\eta^2)\mathcal{L}_t, \\ \epsilon_t & \leq \mathcal{O}(\eta^2)\mathcal{L}_t. \end{aligned}$$

Because a sample path where the loss satisfies Condition 2 occurs with high probability (over random initialization), we have the following result for ReLU networks.

Theorem 1. *Gradient descent with step size $\eta = \mathcal{O}(\lambda_{\min}(\hat{\mathcal{K}}_t))$ on the MSE loss satisfies the recursion below for sufficiently wide, properly initialized ReLU networks:*

$$\mathcal{L}_{t+1} \leq \left(1 - c\eta\lambda_{\min}(\hat{\mathcal{K}}_t)\right)\mathcal{L}_t \quad (7)$$

for an appropriate constant $c > 0$ that depends on width, dataset size, number of layers, and other problem parameters independent of time encoded in the upper bounds of ξ_t/\mathcal{L}_t and ϵ_t/\mathcal{L}_t . Alternatively, we can replace $\lambda_{\min}(\hat{\mathcal{K}}_t)$ in the step size and recursion with $\lambda_{\min}(\mathcal{K})$.

Proof. Directly follows from Lemmas 3 and 4. \square

One could derive time-independent coefficients since $\lambda_{\min}(\hat{\mathcal{K}}_t)$ is close to $\lambda_{\min}(\mathcal{K})$ for all t , for example Theorem 5 in (Allen-Zhu et al., 2019) shows that $\|\hat{\mathcal{K}}_t - \mathcal{K}\|$ is small for all t and can be combined with Matrix-Chernoff techniques to bound eigenvalue deviations. This makes it possible to show linear convergence $\mathcal{L}_T = \mathcal{O}\left((1 - \eta\lambda_{\min}(\mathcal{K}))^T\right)$ and express the admissible constant step sizes in terms of $\lambda_{\min}(\mathcal{K})$. However, we leave the recursion at its current form which gives a stronger and useful bound for the next section.

2.4 SSL with Narrow Networks

Networks used in practice are often much narrower than those required for GD’s trajectory to lie near the vicinity of initialization, and bounds on $\xi_t + \epsilon_t$ or replacement of $\lambda_{\min}(\hat{\mathcal{K}}_t)$ with $\lambda_{\min}(\mathcal{K})$ is not applicable. The former issue is addressed here and we deal with the latter in Section 3.1. Most SSL algorithms build upon using input perturbations (e.g. Π -model, Laine & Aila (2017)) and weight averaging (e.g. mean teacher Tarvainen & Valpola (2017)) to enforce consistency between predictions. Athiwaratkun et al. (2019) analyzed simple versions of these seminal algorithms, illustrating how they effectively penalize the network’s Hessian $\nabla^2 f_\theta$. This effect is equivalent to imposing Lipschitz-continuity on gradients $\|\nabla f_\theta - \nabla f_{\theta'}\| \leq H\|\theta - \theta'\|$, hence smaller smoothness coefficients. Supposing a hard constraint $\nabla^2 f \preceq HI$, we have $\|\nabla f(\theta - \gamma v) - \nabla f(\theta)\| \leq \gamma H v$ for sufficiently small γ . Following the proof of Lemma 4,

$$\xi_t, \epsilon_t \sim \mathcal{L}_t \eta^2 H. \quad (8)$$

This approximation shows that by enforcing small H , SSL variants not only induce a flat landscape near minima often intertwined with generalization, but also affects training, reducing the perturbation terms ξ_t and ϵ_t that otherwise relied on overparametrization to remain small over time.

3 Method

3.1 Convergence Rate Control

We showed that the model’s Gram matrix’ minimum eigenvalue $\lambda_{\min}(\hat{\mathcal{K}}_t) \geq 0$ influences the convergence rate regardless of the architecture or its width. We hence propose to select unlabeled instances \mathcal{X}_u^* from the unlabeled pool \mathcal{X}_U that results in the best problem conditioning, hence the name convergence rate control (CRC). CRC ‘scores’ unlabeled instances based on how much the Gram matrix’ smallest eigenvalue can increase upon labeling:

$$\max_{\mathcal{X}_u \subset \mathcal{X}_U} \min_{i \in |\mathcal{X}_L \cup \mathcal{X}_u|} \lambda_i \left(\hat{\mathcal{K}}^{(T)}(\mathcal{X}_u \cup \mathcal{X}_L, \mathcal{X}_u \cup \mathcal{X}_L) \right). \quad (9)$$

The block $\hat{\mathcal{K}}^{(T)}(x, x') \in \mathbb{R}^{C \times C}$ grows quadratically with the number of classes C , and is replaced by its trace computed as $\tilde{\mathcal{K}}^{(T)}(x, x') = \sum_c \hat{\mathcal{K}}_{cc}^{(T)}(x, x')$ which we numerically found to be an accurate replacement in computing the minimum eigenvalue. Considering only the positive eigenvalues of this approximation consistently achieved higher performance. The solution to Eq. 9 can then be found using dedicated GPU-implementations available in popular DL frameworks. This algorithm is detailed in Alg. 1.

Intuitively, a sample’s label may be most informative when it is near a region separating different classes; however, this does not guarantee that a DNN learns such a decision boundary effectively. Furthermore, it is unclear whether a sample in some other region could better enhance a classifier’s performance when added to the labeled set, especially when considering SSL algorithms which complicate DL analysis. Contrary to the above intuition, Rebuffi et al. (2020) demonstrate how

Algorithm 1 Convergence Rate Control (batch-mode solution to (9))

Inputs: Unlabeled pool \mathcal{X}_U , acquisition size Q , group-size G .
Output: New pool \mathcal{X}_u^* to be labeled.
for $i = 1, \dots, \lceil \mathcal{X}_U \rceil / G$ **do**
 $\mathcal{X}_u^{(i)} \leftarrow G$ unlabeled instances randomly sampled from \mathcal{X}_U .
 $s(\mathcal{X}_u^{(i)}) \leftarrow \lambda_{\min}^+(\mathcal{X}_L \cup \mathcal{X}_u^{(i)})$ using the empirical NTK computed over final layers.
end for
Store Q/G highest groups: $i_1^*, \dots, i_{Q/G}^* \leftarrow \arg \max(s)$.
Return $\mathcal{X}_u^* \leftarrow \mathcal{X}_u^{(i_1^*)} \cup \dots \cup \mathcal{X}_u^{(i_{Q/G}^*)}$

a DNN trained on a SSL objective (Laine & Aila, 2017) learns a decision boundary using only 4 manually selected pivot points not on the class-separating region. In an attempt to understand the abstruse behavior of DNNs, we visualize in Figure 1 how the classifier’s decision boundary progressively forms near low-density regions as CRC enlarges the labeled set.

3.2 Myopic vs. Batch-Mode Active Learning

Myopic AL policies refer to algorithms that score unlabeled instances based on their individual importance. Considering how an expert annotator ‘in-the-loop’ must label queried samples, it is desirable that an AL algorithm queries large batches based on their collective importance. Myopic policies usually degrade in performance as the acquisition size Q increases, as they may repetitively query identical instances (Kirsch et al., 2019), and it has been of great interest in designing a computationally efficient batch-AL algorithm. CRC (Alg. 1) is a batch-mode AL algorithm since it computes λ_{\min} over groups of unlabeled instances \mathcal{X}_u and the labeled set, where $Q = 1$ would be a myopic policy which is trivially optimal for acquisition size 1.

A dataset \mathcal{X} with duplicate instances is called degenerate, or equivalently any non-degenerate set \mathcal{X} satisfies $\|x - x'\| > 0$ for every pair $(x, x') \in \mathcal{X}, x \neq x'$. Consider multisets \mathcal{X} , i.e. sets \mathcal{X} can have duplicate elements: $\mathcal{X} \neq \mathcal{X} \cup \{x\}$ for any $x \in \mathcal{X}$. The statement below shows that CRC never queries identical samples or those already in the labeled set if a non-degenerate candidate exists in the search space. Proposition 2 alone resolves issues with many AL algorithms that acquire identical samples on repeated datasets such as ‘repeated MNIST’ (Kirsch et al., 2019).

Proposition 2 (CRC finds non-degenerate solutions). *Suppose $x_i \neq x_j \Rightarrow \hat{\mathcal{K}}^{(T)}(x_i, \cdot) \neq \hat{\mathcal{K}}^{(T)}(x_j, \cdot)$ for every $x_i, x_j \in \mathcal{X}_L \cup \mathcal{X}_U$. If there exists a non-degenerate solution $\mathcal{X}_u^* \subset \mathcal{X}_U$,*

$$\lambda_{\min}(\mathcal{X}_L \cup \mathcal{X}_u^*) > \lambda_{\min}(\mathcal{X}_L \cup \mathcal{X}_u^* \setminus \{x_i\} \cup \{x_j\}), \quad (10)$$

for every $x_i, x_j \in \mathcal{X}_L \cup \mathcal{X}_u^, x_i \neq x_j$.*

Proof. All eigenvalues computed over non-degenerate sets $\mathcal{X}_L \cup \mathcal{X}_u^*$ are non-zero since the row vectors in $\hat{\mathcal{K}}^{(t)}(\mathcal{X}_L \cup \mathcal{X}_u^*)$ are linearly independent. Complemented with the semi-positive definiteness of $\hat{\mathcal{K}}$, LHS > 0 . Since the RHS has duplicate elements in the multiset, at least two row vectors are linearly dependent and $\hat{\mathcal{K}}^{(t)}$ is non-invertible, implying RHS=0. Furthermore, the result holds without loss of generality when the RHS’s arguments are replaced with any degenerate candidate. \square

Remark 1. *Intuitively, the assumption $x_i \neq x_j \Rightarrow \hat{\mathcal{K}}(x_i, \cdot) \neq \hat{\mathcal{K}}(x_j, \cdot)$ means that a high dimensional vector (function’s gradients) is one-to-one on the small and countable domain $\mathcal{X}_L \cup \mathcal{X}_U$. This is true at least in the neighborhood of initialization for ReLU networks as long as not too many neurons are deactivated (Allen-Zhu et al., 2019) or for another class of networks Du et al. (2019).*

To cope with the combinatorial complexity of the outer-maximization in Eq. 9, we randomly sample candidate groups \mathcal{X}_u without replacement. Note that our batch approximation is quite different from the ϵ -greedy approach used by most batch mode AL algorithms (Sener & Savarese, 2017; Kirsch et al., 2019); a greedy approximation of CRC could iteratively add singleton candidates x_u that maximize the resulting minimum eigenvalue for Q iterations, requiring $O(UQ)$ eigen-decompositions instead of our $O(Q/G)$, and the selected batch may be highly sub-optimal, deviating significantly from the optimal batch’s (max-min) score.

Table 1: Effect of different group sizes with $Q = 100$.

# Labeled	200	300	400	500
$G = 2$	84.72 ± 0.96	87.11 ± 1.14	87.83 ± 0.17	88.30 ± 0.30
$G = 5$	82.55 ± 3.21	84.13 ± 2.64	87.24 ± 2.42	87.66 ± 1.33
$G = 10$	83.38 ± 1.14	85.71 ± 1.50	88.07 ± 0.06	88.36 ± 0.71
$G = 100$	83.31 ± 2.17	86.49 ± 1.47	86.76 ± 2.56	88.49 ± 1.43

Randomization significantly reduces the search space, potentially yielding highly sub-optimal solutions, and we introduce a hyperparameter G such that G divides Q , and search over candidate groups $|\mathcal{X}_u| = G$, selecting Q/G groups at each acquisition step. The group size controls whether the outer maximization is solved more accurately ($G = 1$) without considering the collective significance of a group, or the inner-minimization (cubic in group size using Power method) incorporates the collective importance of all queried samples ($G = Q$) at the expense of a smaller search space, by a constant multiplicative factor negligible compared to the combinatorially large search space. We show in Table 1 that G doesn’t affect the performance as long as $G > 1$, and the hyperparameter can be chosen based on the runtime/memory resulting from implementation differences; inefficient batch-gradient computations in standard autograd packages make each step slower with larger G , whereas larger G requires less eigen-decompositions.

3.3 Practical Considerations

Each entry in $\hat{\mathcal{K}}_t = \sum_l \hat{\mathcal{K}}_t^{(l)}$ requires computing the gradient over all layers. Every layer’s Gram matrix $\hat{\mathcal{K}}_t^{(l)}$ is semi-positive definite, and $1 - c\eta\lambda_{\min}(\hat{\mathcal{K}}_t) \leq 1 - c\eta\lambda_{\min}(\hat{\mathcal{K}}_t^L)$. Therefore, convergence in Theorem 1 can also be established with respect to using just the last layer’s Gram matrix which significantly reduces computation.

We compared the performance of CRC when replacing $\lambda_{\min}(\hat{\mathcal{K}}_t)$ with $\lambda_{\min}(\hat{\mathcal{K}}_t^L)$ in Table 2. Recall that the intuition behind CRC is in estimating and improving the classifier’s training dynamics over to-be-labeled samples. Raghu et al. (2017) show that identical architecture-training schemes over different realizations of random initialization tend to learn similar representations towards the last few layers, but drastically different features in intermediate layers. Because we consider an experimental setting where a network is trained from scratch between acquisition steps, using gradients of intermediate layers can actually hurt the next acquisition step’s training dynamic estimate. This phenomenon is highlighted from last-CRC’s outperforming full-CRC.

Table 2: CRC performances when NTK is computed over last vs. all layers with $Q = 50$ at $G = 5$.

# Labeled	100	150	200
Last	78.41 ± 3.16	83.67 ± 3.24	85.67 ± 1.31
Full	71.26 ± 3.92	78.13 ± 4.32	79.10 ± 3.64

3.4 Relation to Gradient-based Methods

The proposed algorithm can be interpreted as measuring the importance of unlabeled instances by how much they would change a model’s parameters. Two AL algorithms are similar in this manner in that they seek to label instances which affect the model the most: expected gradient length (EGL) (Huang et al., 2016) and BADGE (Ash et al., 2020). EGL first computes the gradient of the cross-entropy loss over all unlabeled instances, replacing the ground truth target with an expectation over a posterior distribution determined by the trained model, then selects instances with the greatest norm. BADGE uses an embedding of the loss’ gradients using predicted classes, computed over the parameters in just the final layer, and uses kmeans++ to enforce diversity. Nonetheless, both algorithms score candidate unlabeled samples based on their marginal importance and do not measure the collective influence of the labeled set.

Table 3: Pseudo-AL: Mean Teacher ($R_0 = 12, R = 2$) and FixMatch ($R_0 = 1, R = 1$) achieved 50.2% and 55.9% accuracy on SVHN and CIFAR10, respectively, on the initial labeled set. See appendix for performances marked with *.

Accuracy (%) # Labeled per class	SVHN					CIFAR10		
	14	16	18	20	22	2	3	4
Random	58.40±6.04	67.96±8.51	83.12±6.60	86.01±6.58	90.75±2.57	83.31±10.80	86.20±7.14	93.28±0.40
Entropy	52.08±3.58	70.98±7.63	78.25±3.18	88.99±2.25	91.23±0.62	74.03±5.88	87.50±4.15	93.80±1.16
Confidence	53.14±3.37	58.02±6.77	76.2±2.66	86.92±7.15	90.25±0.19	69.22±12.75	74.65±14.14	70.86±3.95*
EGL	50.81±6.36	67.73±8.99	73.63±8.54	78.15±3.29	82.64±1.86	83.33±4.01	84.49±4.57	80.65±5.30*
CRC [†]	58.74±6.37	76.09±7.06	84.36±8.10	90.87±0.60	91.39±0.49	89.41±1.57	91.41±1.84	94.09±1.12

4 Experiments

4.1 Implementation Details

There is no standard experimental design for benchmarking AL algorithms, let alone for ASSL. We adopt all SSL-related configurations from (Oliver et al., 2018), e.g. WRN-28-2 architecture. Following most AL experimental setups, we train the classifier from scratch between acquisitions. While this requires substantially more computational resources, we believe this is the most fair comparison between AL algorithms for the following reasons. First, classification models trained on different datasets may benefit from different time horizons. However, it is difficult to determine the best number of training epochs for the initial and subsequent acquisitions that work well across all ASSL algorithms. Another reason is that a good AL algorithm should construct the dataset such that a randomly initialized model can also perform well on the newly updated dataset for practical applicability; if the dataset benefits only one particular model’s initial weights, the labeled dataset cannot be recycled to train another classification model. In fact, we show in the Appendix that most AL algorithms have poor transferrability properties, where labeled data selected using one model is not as useful when training another model.

We compare CRC’s performance against other AL schemes across several SSL algorithms and publicly-available PyTorch implementations on 3 datasets: SVHN¹ CIFAR10², CIFAR100³. Mean teacher (MT, Tarvainen & Valpola (2017)) enforces consistency between the model trained using SGD and an exponential moving average (teacher) of the model’s weights. In short, FixMatch (Sohn et al., 2020) enforces consistency between a classification model’s predictions on perturbed inputs which effectively yields a more robust model with small Jacobian norm (Athiwaratkun et al., 2019) in junction with other SSL algorithms including MT. The hyperparameters in FixMatch were kept the same across different dataset sizes in their original report, making our experimental comparisons convenient and fair.

The initial pool of labeled instances significantly affected the downstream SSL task and subsequent AL queries, especially for uncertainty-based algorithms (see section 4.2). It is practical to assume that a model would initially have access to a small pool of labeled images with an equal number of classes. For robustness of performance, we randomly sampled Q_0 images from each class in the first acquisition step and used the model that attained median performance across 5 and 3 trials for experiments in sections 4.3.1 and 4.3.2, respectively. At each acquisition step, the classification network was trained until either its accuracy saturated and did not improve for 50/100/ ∞ epochs or 350/600/512 epochs was reached for CIFAR10/100/SVHN before querying for labels. All experiments were repeated 3 times with mean \pm std performances reported unless stated otherwise.

4.2 Baseline Algorithms

Both AL and SSL algorithms demand much more time than standard supervised learning, and an extensive comparison of all ASSL combinations is beyond our compute availability. We resort to comparing the proposed algorithm with 3 other AL algorithms, 2 of which scores unlabeled instances

¹Mean Teacher: <https://github.com/perrying/realistic-ssl-evaluation-pytorch>

²FixMatch: two different versions of <https://github.com/kekmodel/FixMatch-pytorch>. The early version updated batch stats in the EMA model and was used for Section 4.3.2, whereas a later version that didn’t update batch stats was used for Section 4.3.1

³FixMatch: <https://github.com/LeedoYup/FixMatch-pytorch>

based on how much they reduce a model’s uncertainty, and the other because of its similarity to CRC. Uncertainty-based AL (Wang & Shang, 2014) is one of the simplest DL-based AL algorithm that selects the unlabeled instance with lowest confidence in its prediction: $\min_{\{x \in \mathcal{X}_U\}} \max_y f_{\theta,y}(x)$. In the same work, Wang & Shang (2014) proposed to also use entropy as a measure of the model’s uncertainty in unlabeled samples. Entropy is currently the state-of-the-art AL algorithm reported in the purely-supervised (non-SSL) setting. EGL (Huang et al., 2016) retrieves instances that modify a model the most: $\max_{\{x \in \mathcal{X}_U\}} \mathbb{E}_{y \sim \hat{p}(\cdot; x, \theta)} [\|\nabla_{\theta} H(y, f_{\theta}(x))\|^2]$ where $\hat{p}(y; x_i, \theta) = \sigma(f_{\theta}(x_i))_y$ is the model’s confidence in class y , σ is softmax, and H is the cross entropy function.

4.3 Results

4.3.1 Balanced Classes

Modern SSL algorithms we consider achieve outstanding performance with extremely few labeled data, and the performance gain of AL schemes in the low-data regime is of interest. One issue arises from this low-data setting: class-imbalance. While SSL algorithms are typically tested with respect to passive (random) sampling, this falls under what we call ‘pseudo-AL’ where the labeled dataset, and consequently unlabeled set, is guaranteed to have the same number images per class. In contrast, AL seeks to query data whose label is unknown, and sampling algorithms cannot guarantee balanced classes simply because the classes are unknown, which would defeat the purpose of AL. AL benchmarks that do not consider SSL typically query large numbers of labeled images, and class-imbalance does not affect classification performance as much as in the low-data regime considered in our work. We first compare ASSL algorithms on pseudo-AL in Table 3 where the algorithms have access to different pools of unlabeled images corresponding to different, but unknown classes, to control performance degradation with respect to class-imbalance. Here, R_0 and R denote the number of images sampled per class in the initial and subsequent acquisitions where $Q = RC$. CRC searched over candidate groups of size $G = Q$ that contained R images of each class.

4.3.2 Active Semi-Supervised Learning

Here we report the performances of SSL algorithms in Tabs. 4, 5, and 6 when Q images were acquired under the more practical scenario where class-balance cannot be enforced. As described earlier, only the first acquisition step randomly sampled Q_0/C images per class for a total of Q_0 images. For reference, the implementations used for each experiment achieve the following average accuracies: SVHN (100 per class) - 93.52%, CIFAR10 (25 per class) - 87.33%, and CIFAR100 (40 per class) - 48.96% with random sampling in the pseudo-AL setting (balanced classes). Different levels of class-imbalance result in larger performance variance, which is especially critical in the low-data regime.

Table 4: Mean Teacher on SVHN with $Q_0 = 120$, $Q = 20$. CRC used $G = 20$.

Accuracy (%) # Labeled	SVHN			
	140	160	180	200
Random	56.03±5.88	66.48±12.53	73.46±1.73	89.20±1.08
Entropy	53.36±4.90	62.17±11.97	80.87±6.15	89.09±1.45
Confidence	51.40±4.62	70.75±12.63	63.06±9.62	82.67±4.87
EGL	52.16±4.57	58.88±6.74	62.52±3.31	73.46±2.37
CRC [†]	55.52±9.91	74.66±1.31	83.50±8.37	89.39±1.78

Table 5: FixMatch on CIFAR100 with $Q_0 = 200$ and $Q = 50$. Here we compare only CRC with random sampling due to the arduous computation of FixMatch on CIFAR100.

Accuracy (%) # Labeled	CIFAR100				
	250	300	350	400	450
Random	41.45±1.04	44.57±0.74	45.19±0.91	49.35±1.55	51.20±0.83
CRC [†]	41.87±1.45	45.27±0.59	47.04±0.50	50.16±0.37	52.40±0.93

Table 6: FixMatch accuracy on CIFAR10 using $Q \in \{50, 100\}$.

Accuracy (%) # Labeled	Q=50					Q=100				
	100	150	200	250	300	200	300	400	500	600
Random	69.81±4.77	82.14±2.30	82.41±0.68	84.98±2.32	84.92±0.73	85.04±1.53	87.09±1.25	87.57±0.57	87.92±0.47	87.37±2.18
Entropy	72.43±8.21	82.41±2.89	83.38±1.93	84.86±1.83	86.42±0.95	85.51±1.47	86.89±0.47	86.87±1.22	88.27±0.30	88.44±1.17
Confidence	52.54±7.71	49.55±7.77	50.67±3.15	45.04±8.25	53.44±8.75	77.05±4.66	78.29±5.55	73.68±5.12	73.69±2.50	75.98±3.29
EGL	57.18±7.41	56.67±10.53	68.76±12.57	74.47±12.32	76.67±7.43	79.95±3.11	80.41±2.77	81.20±5.10	82.62±0.36	83.55±3.36
CRC [†]	78.41±3.16	83.67±3.24	85.67±1.31	86.88±0.87	87.01±0.28	83.38±1.14	85.71±1.50	88.08±0.06	88.37±0.71	89.35±0.79

In contrast to standard (non-SSL) AL settings that consider much larger query sizes, the small query size in ASSL significantly impacts the class distribution, resulting in occasional performance drop for certain acquisition strategies. Entropy repeatedly achieved state-of-the-art performance (Gissin & Shalev-Shwartz, 2019; Wang et al., 2016; Ash et al., 2020) in AL despite its simplicity, and our experiments show the same holds for ASSL. CRC performed comparable or better than all considered baselines across all datasets and query sizes. Furthermore, while CRC and EGL both score candidates by estimating how much they would affect the model’s training dynamics, only CRC outperformed random sampling. Our results suggest that actively enlarging the labeled set can reduce the sample complexity in the SSL setting.

Existing DL-based AL algorithms have performed comparably to random sampling when using large query sizes, and our experiments show the same for entropy and CRC with $Q = 100$ in the ASSL setting. A proper AL algorithm should achieve higher performance at the same number of labeled samples when using smaller acquisition sizes, as it would be querying for labels more often; however, only CRC satisfied this property. EGL’s low performance had been reported on image classification tasks (Gissin & Shalev-Shwartz, 2019; Sener & Savarese, 2017; Ducoffe & Precioso, 2018) and is confirmed in ASSL. Retraining networks from scratch may have had negative influence on EGL, similar to how it adversely affected full-CRC. We attribute confidence’s low performance to the poor calibration of DNNs (Guo et al., 2017), inadequately capturing the model’s uncertainty on unlabeled instances. A successful application of confidence-based query may require incorporating calibration while training classification networks or before performing such queries.

5 Conclusion

This work motivated the combination of AL with SSL, using the former for optimization and latter objective to restrict the hypothesis space to those that generalize well. We then proposed an AL algorithm inspired by the NTK, and demonstrated that querying unlabeled data based on their resulting convergence rate significantly improves sample efficiency. To the best of our knowledge, this work is the first practical application of NTK outside of supervised learning, where it has been shown that the true NTK is inferior to its DNN counterpart. In contrast to most DL-based AL experiments which use relatively small networks, this work demonstrates that DL can benefit from AL using modern architectures. Our algorithm outperformed uncertainty-based AL algorithms and another algorithm with a similar goal of maximizing the model’s change. The proposed algorithm’s superiority was shown in the batch-AL setting, where an optional hyperparameter can be used to control the trade-off between computational complexity and performance.

Our CRC algorithm is developed under the assumption that a well-optimized network $f^{(\infty)}$ induced by the SSL objective is a good approximation of a model f^* that generalizes well. Incorporating the interplay between AL and SSL seems promising in further reducing the sample complexity, designing either an SSL algorithm best fit for some fixed AL algorithm or a joint ASSL scheme. For example, CRC provides an estimate on the number of epochs required for convergence, and a learning rate schedule best fit for the estimated time horizon could be used (Ge et al., 2019). As a preliminary demonstration, we show how well CRC’s score reflects the time horizon til convergence in the Appendix.

CRC enjoys several properties that aren’t present in other AL algorithms or is at least not obvious. First, CRC scores the value of labeling data over a combination of already-labeled data and candidate unlabeled data, explicitly consolidating existing labeled data. Moreover, CRC is a batch AL algorithm that provably selects distinct samples, a property which may be lost by other algorithms upon greedy approximations. The proposed algorithm is also interesting in that it is a kernel-based

sampling scheme. Kernels are excellent models of data distributions, and CRC’s construction of a kernel using DL suggests a new direction for AL research.

The proposed CRC algorithm can be extended in several directions, applying generalization guarantees characterized by the NTK to an online (streaming) setting where unlabeled instances cannot be stored. Another exciting direction to pursue would be to use the True NTK (Arora et al., 2019; Novak et al., 2020) to estimate the training dynamics once their performance attains that of finite-width networks. Lastly, AL algorithms could be combined into one AL algorithm to improve their marginal performances, similar to how FixMatch modifies a combination of several seminal SSL algorithms.

References

- Allen-Zhu, Z., Li, Y., and Song, Z. A convergence theory for deep learning via over-parameterization. *arXiv preprint arXiv:1811.03962*, 2019.
- Arora, S., Du, S. S., Hu, W., Li, Z., Salakhutdinov, R. R., and Wang, R. On exact computation with an infinitely wide neural net. In Wallach, H., Larochelle, H., Beygelzimer, A., d’Alché-Buc, F., Fox, E., and Garnett, R. (eds.), *Advances in Neural Information Processing Systems 32*, pp. 8141–8150. Curran Associates, Inc., 2019.
- Ash, J. T., Zhang, C., Krishnamurthy, A., Langford, J., and Agarwal, A. Deep batch active learning by diverse, uncertain gradient lower bounds. In *International Conference on Learning Representations*, 2020.
- Athiwaratkun, B., Finzi, M., Izmailov, P., and Wilson, A. G. There are many consistent explanations of unlabeled data: Why you should average. In *International Conference on Learning Representations*, 2019.
- Balcan, M.-F., Hanneke, S., and Vaughan, J. The true sample complexity of active learning. *Machine Learning*, 80:111–139, 09 2010. doi: 10.1007/s10994-010-5174-y.
- Ben-David, S., Blitzer, J., Crammer, K., Kulesza, A., Pereira, F., and Vaughan, J. A theory of learning from different domains. *Machine Learning*, 79:151–175, 2010.
- Berthelot, D., Carlini, N., Goodfellow, I., Papernot, N., Oliver, A., and Raffel, C. Mixmatch: A holistic approach to semi-supervised learning. *arXiv preprint arXiv:1905.02249*, 2019.
- Du, S., Lee, J., Li, H., Wang, L., and Zhai, X. Gradient descent finds global minima of deep neural networks. volume 97 of *Proceedings of Machine Learning Research*, pp. 1675–1685, Long Beach, California, USA, 09–15 Jun 2019. PMLR.
- Ducoffe, M. and Precioso, F. Adversarial active learning for deep networks: a margin based approach. *arXiv preprint arXiv:1802.09841*, 2018.
- Ge, R., Kakade, S. M., Kidambi, R., and Netrapalli, P. The step decay schedule: A near optimal, geometrically decaying learning rate procedure for least squares. In Wallach, H., Larochelle, H., Beygelzimer, A., d’Alché-Buc, F., Fox, E., and Garnett, R. (eds.), *Advances in Neural Information Processing Systems 32*, pp. 14977–14988. Curran Associates, Inc., 2019.
- Gissin, D. and Shalev-Shwartz, S. Discriminative active learning. *arXiv preprint arXiv:1907.06347*, 2019.
- Göpfert, C., Ben-David, S., Bousquet, O., Gelly, S., Tolstikhin, I., and Uner, R. When can unlabeled data improve the learning rate? In *COLT*, 2019.
- Guo, C., Pleiss, G., Sun, Y., and Weinberger, K. Q. On calibration of modern neural networks. In *Proceedings of the 34th International Conference on Machine Learning - Volume 70, ICML’17*, pp. 1321–1330. JMLR.org, 2017.
- He, H., Huang, G., and Yuan, Y. Asymmetric valleys: Beyond sharp and flat local minima. In Wallach, H., Larochelle, H., Beygelzimer, A., d’Alché-Buc, F., Fox, E., and Garnett, R. (eds.), *Advances in Neural Information Processing Systems*, volume 32, pp. 2553–2564. Curran Associates, Inc., 2019.

- Huang, J., Child, R., Rao, V., Liu, H., Satheesh, S., and Coates, A. Active learning for speech recognition: the power of gradients. 12 2016.
- Jacot, A., Gabriel, F., and Hongler, C. Neural tangent kernel: Convergence and generalization in neural networks. In Bengio, S., Wallach, H., Larochelle, H., Grauman, K., Cesa-Bianchi, N., and Garnett, R. (eds.), *Advances in Neural Information Processing Systems 31*, pp. 8571–8580. Curran Associates, Inc., 2018.
- Kirsch, A., van Amersfoort, J., and Gal, Y. Batchbald: Efficient and diverse batch acquisition for deep bayesian active learning. In Wallach, H., Larochelle, H., Beygelzimer, A., d'Alché-Buc, F., Fox, E., and Garnett, R. (eds.), *Advances in Neural Information Processing Systems 32*, pp. 7026–7037. Curran Associates, Inc., 2019.
- Laine, S. and Aila, T. Temporal ensembling for semi-supervised learning. In *ICLR (Poster)*. Open-Review.net, 2017.
- Lee, D.-H. Pseudo-label : The simple and efficient semi-supervised learning method for deep neural networks. *ICML 2013 Workshop : Challenges in Representation Learning (WREPL)*, 07 2013.
- Lee, J., Xiao, L., Schoenholz, S. S., Bahri, Y., Novak, R., Sohl-Dickstein, J., and Pennington, J. Wide neural networks of any depth evolve as linear models under gradient descent, 2019.
- Lopez-Paz, D., Bottou, L., Schölkopf, B., and Vapnik, V. Unifying distillation and privileged information, 2016.
- Massart, P. and Nédélec, E. Risk bounds for statistical learning. *The Annals of Statistics*, 34, 10 2006. doi: 10.1214/009053606000000786.
- Nitanda, A. and Suzuki, T. Optimal rates for averaged stochastic gradient descent under neural tangent kernel regime, 06 2020.
- Novak, R., Xiao, L., Hron, J., Lee, J., Alemi, A. A., Sohl-Dickstein, J., and Schoenholz, S. S. Neural tangents: Fast and easy infinite neural networks in python. In *International Conference on Learning Representations*, 2020.
- Oliver, A., Odena, A., Raffel, C. A., Cubuk, E. D., and Goodfellow, I. Realistic evaluation of deep semi-supervised learning algorithms. In Bengio, S., Wallach, H., Larochelle, H., Grauman, K., Cesa-Bianchi, N., and Garnett, R. (eds.), *Advances in Neural Information Processing Systems 31*, pp. 3235–3246. Curran Associates, Inc., 2018.
- Raghu, M., Gilmer, J., Yosinski, J., and Sohl-Dickstein, J. Svcca: Singular vector canonical correlation analysis for deep learning dynamics and interpretability. In Guyon, I., Luxburg, U. V., Bengio, S., Wallach, H., Fergus, R., Vishwanathan, S., and Garnett, R. (eds.), *Advances in Neural Information Processing Systems 30*, pp. 6076–6085. Curran Associates, Inc., 2017.
- Rebuffi, S.-A., Ehrhardt, S., Han, K., Vedaldi, A., and Zisserman, A. Semi-supervised learning with scarce annotations. In *Proceedings of the IEEE/CVF Conference on Computer Vision and Pattern Recognition Workshops*, pp. 762–763, 2020.
- Sener, O. and Savarese, S. Active learning for convolutional neural networks: A core-set approach. *arXiv preprint arXiv:1708.00489*, 2017.
- Sohn, K., Berthelot, D., Li, C.-L., Zhang, Z., Carlini, N., Cubuk, E. D., Kurakin, A., Zhang, H., and Raffel, C. Fixmatch: Simplifying semi-supervised learning with consistency and confidence. *arXiv preprint arXiv:2001.07685*, 2020.
- Song, S., Berthelot, D., and Rostamizadeh, A. Combining mixmatch and active learning for better accuracy with fewer labels. *arXiv preprint arXiv:1912.00594*, 2019.
- Tarvainen, A. and Valpola, H. Mean teachers are better role models: Weight-averaged consistency targets improve semi-supervised deep learning results. In Guyon, I., Luxburg, U. V., Bengio, S., Wallach, H., Fergus, R., Vishwanathan, S., and Garnett, R. (eds.), *Advances in Neural Information Processing Systems 30*, pp. 1195–1204. Curran Associates, Inc., 2017.

- Wang, D. and Shang, Y. A new active labeling method for deep learning. In *2014 International joint conference on neural networks (IJCNN)*, pp. 112–119. IEEE, 2014.
- Wang, K., Zhang, D., Li, Y., Zhang, R., and Lin, L. Cost-effective active learning for deep image classification. *IEEE Transactions on Circuits and Systems for Video Technology*, 27(12):2591–2600, 2016.

A Deferred Proofs

We adopt the convention that all gradients are flattened in vector form and use the Euclidean norms to represent their size.

A.1 Derivation of Lemma 1

Lemma 3. *For any DNN architecture with once-differentiable activation functions, gradient descent with step size η follows the recursive relation:*

$$\mathcal{L}_{t+1} \leq \left(1 - \eta \lambda_{\min}(\hat{\mathcal{K}}_t)\right) \mathcal{L}_t + \xi_t + \epsilon_t, \quad (11)$$

where $\xi_t = \int_0^\eta \nabla \mathcal{L}_t^T (\nabla \mathcal{L}_t - \nabla \mathcal{L}(\theta_t - \gamma \nabla \mathcal{L}_t)) d\gamma$ and $\epsilon_t = \frac{1}{2}(f_{\theta_{t+1}} - f_{\theta_t})^2$.

This derivation is mostly from Du et al. (2019), but we make it explicit that their assumptions on activation functions are not necessary for Lemma 3. Let $e_t = y - f_{\theta_t}$. A standard technique with triangular inequality gives

$$\mathcal{L}_{t+1} \leq \mathcal{L}_t + \|f_{\theta_{t+1}} - f_{\theta_t}\|^2 - 2e_t^T (f_{\theta_{t+1}} - f_{\theta_t}). \quad (12)$$

Let $h(\eta) = f(\theta_t - \eta \nabla \mathcal{L}_t)$. By the fundamental theorem of calculus,

$$\begin{aligned} f_{\theta_{t+1}} - f_{\theta_t} &= h(\eta) - h(0) \\ &= \int_0^\eta h'(\gamma) d\gamma = \int_0^\eta h'(0) d\gamma + \int_0^\eta h'(\gamma) - h'(0) d\gamma \end{aligned}$$

Since $h'(0) = -\nabla f(\theta_t) \nabla \mathcal{L}_t = -e \nabla f_{\theta_t}^T \nabla f_{\theta_t} = -e \hat{\mathcal{K}}_t$, we have

$$\begin{aligned} e^T (f_{\theta_{t+1}} - f_{\theta_t}) &= -\eta e^T \hat{\mathcal{K}}_t e + \int_0^\eta h'(\gamma) - h'(0) d\gamma \\ &\leq -\eta \lambda_{\min}(\hat{\mathcal{K}}_t) \mathcal{L}_t + \xi_t. \end{aligned}$$

Substituting into Eq. 12 gives Eq. 11 together with $e_t \int_0^\eta h'(\gamma) - h'(0) d\gamma = \int_0^\eta \nabla \mathcal{L}_t^T (\nabla \mathcal{L}_t - \nabla \mathcal{L}(\theta_t - \gamma \nabla \mathcal{L}_t)) d\gamma$.

A.2 Proof of Lemma 2

Definition 3 (Semi-smooth). *A function g is (α, β) -smooth if*

$$g(y) \leq g(x) + \nabla g(x)^T (y - x) + \alpha \sqrt{g(x)} \|y - x\| + \beta \|y - x\|^2. \quad (13)$$

Definition 4 (Gradient Scale). *A function $g \in C^1(\mathcal{X})$ has gradients ∇g that scale as (μ, M) if*

$$\mu g(x) \leq \|\nabla g(x)\|^2 \leq M g(x), \forall x \in \mathcal{X}. \quad (14)$$

If a function's gradients scale as (μ, M) , we say the gradient scale is bounded.

We will make use of the following property of smooth functions g .

Proposition 3. *If g is (α, β) -smooth,*

$$(\nabla g(y) - \nabla g(x))(y - x) \leq \alpha(\sqrt{g(x)} + \sqrt{g(y)}) \|y - x\| + 2\beta \|y - x\|^2 \quad (15)$$

Proof. Expanding the LHS in terms of x and y then summing their upper bounds gives the inequality. \square

Condition 2. *The MSE loss is (α, β) -smooth and its gradients scale as (μ, M) .*

Lemma 4. *If $\mathcal{L}_t := \mathcal{L}(\theta_t)$ satisfies Condition 2, we have*

$$\begin{aligned} \xi_t &\leq \mathcal{O}(\eta^2) \mathcal{L}_t, \\ \epsilon_t &\leq \mathcal{O}(\eta^2) \mathcal{L}_t. \end{aligned}$$

Proof. Bound on ξ_t Proposition 3 with \mathcal{L} at θ_t and $\theta_t - \gamma \nabla \mathcal{L}_t$ can be used to bound the integrand.

$$(\nabla \mathcal{L}_t - \nabla \mathcal{L}(\theta_t - \gamma \nabla \mathcal{L}_t)) \nabla \mathcal{L}_t \leq \alpha \|\nabla \mathcal{L}_t\| \left(\sqrt{\mathcal{L}_t} + \sqrt{\mathcal{L}(\theta_t - \gamma \nabla \mathcal{L}_t)} \right) + 2\gamma\beta \|\nabla \mathcal{L}_t\|^2.$$

Using the definition of smoothness

$$\mathcal{L}(\theta_t - \gamma \nabla \mathcal{L}_t) \leq \mathcal{L}_t + \gamma \left(\alpha \sqrt{\mathcal{L}_t} \|\nabla \mathcal{L}_t\| - \|\nabla \mathcal{L}_t\|^2 \right) + \beta \gamma^2 \|\nabla \mathcal{L}_t\|^2,$$

and by gradient drift,

$$\leq \left(1 + \gamma(\alpha\sqrt{M} - \mu) + \beta\gamma^2 \right) \mathcal{L}_t. \quad (16)$$

Let $b = (\alpha\sqrt{M} - \mu)/2\beta$ and $c = 1/\beta - b^2$.

$$\sqrt{\mathcal{L}_t} + \sqrt{\mathcal{L}(\theta_t - \gamma \nabla \mathcal{L}_t)} \leq \sqrt{\mathcal{L}_t} \left(1 + \sqrt{\beta} \left(\gamma + |b| + \sqrt{|c|} \right) \right) =: \sqrt{\mathcal{L}_t} \left(\sqrt{\beta}\gamma + c' \right)$$

by the triangle inequality. Again, $\|\nabla \mathcal{L}_t\|^2 \leq M\mathcal{L}_t$, and we have a bound on the integrand as

$$\begin{aligned} \alpha \|\nabla \mathcal{L}_t\| \left(\sqrt{\mathcal{L}_t} + \sqrt{\mathcal{L}(\theta_t - \gamma \nabla \mathcal{L}_t)} \right) + 2\gamma\beta \|\nabla \mathcal{L}_t\|^2 &\leq \left(\alpha\sqrt{M} \left(\sqrt{\beta}\gamma + c' \right) + 2\gamma\beta M \right) \mathcal{L}_t \\ &=: (a'\gamma + c'') \mathcal{L}_t \end{aligned}$$

$$\Rightarrow \xi_t \leq \mathcal{L}_t \int_0^\eta (a'\gamma + c'') d\gamma = O(\eta^2) \mathcal{L}_t.$$

where we hide constants that depend on the architecture and dataset size.

Bound on ϵ_t It is sufficient that $\epsilon_t \leq (a\eta^2 + \lambda_{\min}\eta) \mathcal{L}_t$ for any a so that \mathcal{L}_t is guaranteed to decrease for small η . This proof is quite involved and relies on analytic expressions for ReLU networks. To this end, we follow the setting in Allen-Zhu et al. (2019) and WLOG fix the last layer's weights as B , denoting pre- and post- activations by g^l, h^l respectively and an 'active-indicator' matrix $D^l \in \mathbb{R}^{d \times d}$, $D_{k,k}^l = \mathbf{1} \{g_{k,k}^l \geq 0\}$, and weight matrices $W_l \in \mathbb{R}^{d \times d}$ for each layer $l \in [L]$, where d denotes the width of the hidden layers and L is the number of layers.

Notice that for ReLU networks, we can write the post-activations at every layer as $h_{t+1}^l - h_t^l = D_{t+1}^l W_{t+1} h_{t+1}^{l-1} - D_t^l W_t h_t^{l-1}$.

Proposition 4 (Distributive diagonal matrices). *There exists $\tilde{D} = (\tilde{D}^1, \dots, \tilde{D}^L)$ with $\tilde{D}^l \in [-1, 1]^{d \times d}$ for every l such that*

$$D_{t+1}^l W_{t+1} h_{t+1}^l - D_t^l W_t h_t^l = \left(D_t^l + \tilde{D}^l \right) \left(W_{t+1}^l h_{t+1}^{l-1} - W_t^l h_t^{l-1} \right).$$

The above proposition follows from case-by-case considerations of ReLU activations, see Proposition 11.3 in Allen-Zhu et al. (2019).

Proposition 5 (Linear expansion of post-activations). *There exists some $\tilde{D}^l \in [-1, 1]^{d \times d}$ at each l such that*

$$h_{t+1}^l - h_t^l = -\eta \sum_{r=1}^l \left(D_t^l + \tilde{D}^l \right) W_t^l \dots W_t^{r+1} \left(D_t^r + \tilde{D}^r \right) \times (\nabla_{W_t^r} \mathcal{L}_t) h_{t+1}^{r-1}$$

The following proposition due to Allen-Zhu et al. (2019) (Lemma 8.6b and Lemma 7.1, respectively) gives bounds on the first line on the RHS and last term:

Proposition 6. *For every $l \in [L]$ and $r \in [l]$,*

$$\left\| \left(D_t^l + \tilde{D}^l \right) W_t^l \dots W_t^{r+1} \left(D_t^r + \tilde{D}^r \right) \right\| \leq O(\sqrt{L}) \|h_{t+1}^{r-1}\| \leq o(1).$$

Applying Cauchy-Schwartz inequality and the fact that norm of sums \leq sum of norms to Propositions 4 and 5,

$$\|f_{\theta_{t+1}} - f_{\theta_t}\| = \|B(h_{t+1}^L - h_t^L)\|, \leq \eta O(L^{1.5} \sqrt{d}) \|\nabla \mathcal{L}_t\|.$$

Since $\|\nabla \mathcal{L}_t\| \leq \sqrt{M\mathcal{L}_t}$,

$$\epsilon_t = \|f_{\theta_{t+1}} - f_{\theta_t}\|^2 \leq O(L^3 d M) \eta^2 \mathcal{L}_t = O(\eta^2) \mathcal{L}_t. \quad (17)$$

□

B Additional Experiments

B.1 Experimental Details

Performances marked with *, for example EGL’s and Confidence’s last query step which performed worse than the previous step, were re-confirmed by fixing the dataset for each of the 3 trials and averaging performance over 2 trials to disentangle performance variance $V(e) = \mathbb{E}[V(e|\mathcal{A}, \mathcal{D})] \approx 1/M \sum_{m \in \{1, \dots, M\}} V(e|\mathcal{A}, \mathcal{D}_m)$ due to the acquired datasets $\mathcal{D}_1 \dots, \mathcal{D}_M$ (AL algorithm) from training instability of SSL algorithms A : $\frac{1}{M} \sum_m V(e|\mathcal{A}_m, \mathcal{D})$ on a fixed dataset \mathcal{D} . This is because running the same ERM algorithm on identical architecture and dataset gives different performances e due to an algorithms’ stability (e.g. order of batch sampling) and initialization. As the dataset size grows, training variance becomes more stable presumably due to SSL being stable when the labeled set is large, and we observed that each of the two trials on a fixed dataset was not as large as the inter-dataset performance, e.g. differences among $(e|\mathcal{D}_1), (e|\mathcal{D}_2), (e|\mathcal{D}_3)$. Hence, confidence and EGL both were observed to occasionally drop in performance with increasing training data. The cause of performance degradation was usually high performance instability, reaching the early-stopping criterion of saturated performance. Performance instability is more of a problem for SSL than standard SL settings, possibly inherent due to the smaller labeled set size or a limitation of current algorithms.

For ASSL, $G > 1$ was set only considering the memory and computation time and was not selected based on performance: SVHN $G = 20$ and $G = Q/10$ for CIFAR10 and CIFAR100.

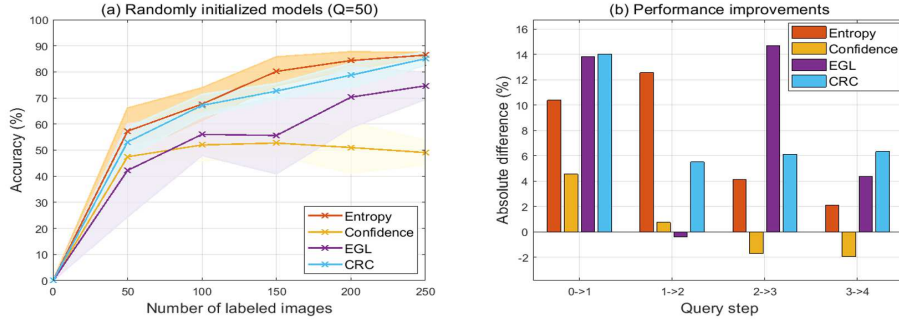


Figure 2: Performances when the initial AL queries were performed using a randomly initialized model. The figure on the right underscores performance gains in consecutive acquisitions.

B.2 Transferrability

An efficient usage of annotation budget would be to construct labeled sets useful to train various models, rather than one specific model. This obviously holds for random sampling, as the queries do not depend on a particular model. To see the transferrability of all considered AL algorithms, modified the realistic experiments so that the first query is performed using the respective AL algorithms with a randomly initialized model, but another model with identical architecture but different initialization seed is trained on the constructed dataset. This is the most primitive form of transferrability, with transferrability to different architectures being more difficult. As shown in Fig. 2, models generally achieved lower performance than when the first query was performed using random sampling, and the initial performance adversely affected all subsequent queries. While entropy and CRC overcome this initial disadvantage after a few query iterations, other baselines tend to underperform random sampling due to this initial disadvantage. This phenomenon has not been reported in previous works, and whether this is an artifact of our ASSL setting deserves future notice.

B.3 Convergence Rate and Time Horizon Prediction

The proposed CRC algorithm is designed to query unlabeled instances that improve the rate of convergence a DNN in the following SSL phase. To see if our algorithm achieves this purpose, we plot the empirical NTK’s minimum eigenvalues used to score unlabeled instance groups against the number of training epochs until the test *loss* reaches its global minimum in Fig. 3 (a) to show

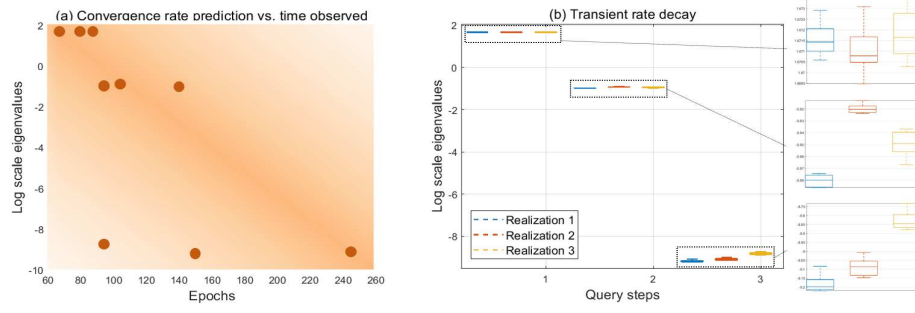


Figure 3: Minimum eigenvalues' distribution in log-scale ($Q = 50$). Left figure shows how informative the minimum eigenvalues are in terms of predicting the number of epochs required for convergence, and right figure illustrates how the minimum eigenvalues' distribution concentrates towards zero. Negative linear slope implies (a) linear convergence as predicted by Lemma 3 and (b) slower convergence rate with increasing labeled set size.

how the minimum eigenvalues are predictive of the time horizon. Global minimum here refers to the value for which the loss never falls below until training completes. We additionally plot how the minimum eigenvalues' distribution progresses with query steps, where Fig. 3 (b) shows that the eigenvalue distribution concentrates towards 0 as the labeled set grows, implying slower convergence rates. A similar observation was made by Nitanda & Suzuki (2020) where the authors showed how the true NTK's eigenvalues concentrate towards zero as the training set size increases, whereas our plot is over a union of labeled and queried groups. This figure illustrates how all candidate datasets will inevitably have eigenvalue distributions concentrated near zero, but the enlarged dataset chosen by CRC will enjoy the fastest convergence rate among all considered candidates.